





Article

Atomistic Insight into the Role of Threonine 127 in the Functional Mechanism of Channelrhodopsin-2

David Ehrenberg ^{1,†}, Nils Krause ^{2,†}, Mattia Saita ¹, Christian Bamann ³, Rajiv K. Kar ⁴ , Kirsten Hoffmann ², Dorothea Heinrich ², Igor Schapiro ⁴ , Joachim Heberle ^{1,*}  and Ramona Schlesinger ^{2,*} 

¹ Experimental Molecular Biophysics, Department of Physics, Freie Universität Berlin, Arnimallee 14, 14195 Berlin, Germany; david.ehrenberg@fu-berlin.de (D.E.); mattiasaita@zedat.fu-berlin.de (M.S.)

² Genetic Biophysics, Department of Physics, Freie Universität Berlin, Arnimallee 14, 14195 Berlin, Germany; NilsKrause@web.de (N.K.); hoffmank@zedat.fu-berlin.de (K.H.); dorothea.heinrich@fu-berlin.de (D.H.)

³ Max-Planck-Institute of Biophysics, Max-von-Laue-Straße 3, 60438 Frankfurt am Main, Germany; christian.bamann@dfg.de

⁴ Fritz Haber Center for Molecular Dynamics Research, Institute of Chemistry, Hebrew University of Jerusalem, Jerusalem 9190401, Israel; rajiv.kar@mail.huji.ac.il (R.K.K.); igor.schapiro@mail.huji.ac.il (I.S.)

* Correspondence: joachim.heberle@fu-berlin.de (J.H.); r.schlesinger@fu-berlin.de (R.S.); Tel.: +49-30-838-56161 (J.H.); +49-30-838-56249 (R.S.)

† These authors contributed equally.

Received: 28 September 2019; Accepted: 12 November 2019; Published: 15 November 2019



Abstract: Channelrhodopsins (ChRs) belong to the unique class of light-gated ion channels. The structure of channelrhodopsin-2 from *Chlamydomonas reinhardtii* (CrChR2) has been resolved, but the mechanistic link between light-induced isomerization of the chromophore retinal and channel gating remains elusive. Replacements of residues C128 and D156 (DC gate) resulted in drastic effects in channel closure. T127 is localized close to the retinal Schiff base and links the DC gate to the Schiff base. The homologous residue in bacteriorhodopsin (T89) has been shown to be crucial for the visible absorption maximum and dark–light adaptation, suggesting an interaction with the retinylidene chromophore, but the replacement had little effect on photocycle kinetics and proton pumping activity. Here, we show that the T127A and T127S variants of CrChR2 leave the visible absorption maximum unaffected. We inferred from hybrid quantum mechanics/molecular mechanics (QM/MM) calculations and resonance Raman spectroscopy that the hydroxylic side chain of T127 is hydrogen-bonded to E123 and the latter is hydrogen-bonded to the retinal Schiff base. The C=N–H vibration of the Schiff base in the T127A variant was 1674 cm^{-1} , the highest among all rhodopsins reported to date. We also found heterogeneity in the Schiff base ground state vibrational properties due to different rotamer conformations of E123. The photoreaction of T127A is characterized by a long-lived P_2^{380} state during which the Schiff base is deprotonated. The conservative replacement of T127S hardly affected the photocycle kinetics. Thus, we inferred that the hydroxyl group at position 127 is part of the proton transfer pathway from D156 to the Schiff base during rise of the P_3^{530} intermediate. This finding provides molecular reasons for the evolutionary conservation of the chemically homologous residues threonine, serine, and cysteine at this position in all channelrhodopsins known so far.

Keywords: channelrhodopsin; resonance Raman; flash photolysis; hybrid QM/MM simulation; electrophysiology

1. Introduction

Channelrhodopsins (ChRs) are members of the group of microbial rhodopsins that are light-gated cation channels. They were originally found in the eyespot of the algae *Chlamydomonas reinhardtii* (Cr),

where they serve to identify optimal light conditions during phototactic movement [1,2]. Typically for rhodopsins, ChRs consist of seven α -helices spanning the membrane and a retinylidene chromophore, which is bound via a Schiff base to a lysine in the core of the protein.

Within the new research field of optogenetics, the coding sequences for light-responsive proteins together with regulating promoters can be introduced into complex organisms and expressed in a tissue-specific way, where cell processes can be triggered. Channelrhodopsin-2 (CrChR2) in neurons can depolarize the nerve cell when illuminated by light of the corresponding wavelength. Although this protein is already frequently used as optogenetic tool, aimed at medical approaches like restoring vision and hearing, the mechanism of action is still not completely understood. Comparison to related microbial rhodopsins where individual positions in the protein sequences are highly conserved could guide our approach towards mechanistically important amino acid residues which have demonstrated effects on photocycle kinetics, activity, and/or structural stability upon mutation.

Decades ago, the Khorana group investigated the role of threonines in the proton pump bacteriorhodopsin (bR) from *Halobacterium salinarum*. In that study, the T89V variant exhibited a blueshift of 146 nm of the visible absorption spectrum without impairing proton pumping [3]. It was concluded from FTIR and time-resolved absorption spectroscopy in the visible range that T89 exerts steric constraints during isomerization of the chromophore and is part of a hydrogen-bonded network including a water molecule and the residues Y185 and D212 [4]. Years later, the same group demonstrated that the hydroxyl group of T89 interacts with the protonated Schiff base in light-adapted bR and influences proton transfer to D85 during the photocycle [5]. However, from X-ray structures [6,7], it became apparent that the OH group of T89 forms a hydrogen bond to an oxygen of the side chain of D85 rather than to the Schiff base. It was concluded from polarized FTIR spectroscopy that the isomerization of the chromophore after light excitation leads to a shortening of the hydrogen bond between T89 and D85, indicating an interconnection to the Schiff base [8]. This tight complex persists from the K intermediate until the M intermediate [9].

The hydroxylic amino acid side chain of T89 of bR is conserved in many channelrhodopsins. The corresponding residue T127 of CrChR2 is located in immediate vicinity to the retinal Schiff base (Figure 1), with a distance of 3.7 Å of the threonine oxygen to the Schiff base nitrogen in the crystal structure. Other channelrhodopsins carry a serine [10] or a cysteine at this position. The latter appears in CaChR1 (from *Chlamydomonas augustae*) and CyChR1 (from *Chlamydomonas yellowstonensis*) [11]. Even anion-conducting channelrhodopsins, which do not conserve E123, have a threonine or a cysteine at this position [12].

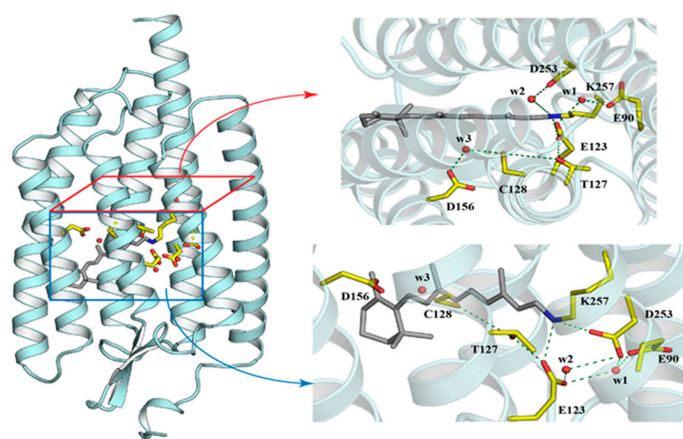


Figure 1. X-ray crystallographic structure of *Chlamydomonas reinhardtii* channelrhodopsin-2 (CrChR2) (PDB: 6EID [10]). The protonated Schiff base of retinal and the side chains of key residues are shown as grey and yellow sticks, respectively. Water molecules are shown as red spheres. Dashed lines indicate hydrogen-bonding interaction.

In CrChR2, the residue T127 is connected via a hydrogen bond to E123, the homologous residue of D85 in bR [10]. The protonation state of E123 is not clear, but nearby ionized D253 serves as the acceptor of the Schiff base proton during the rise of the P₂³⁹⁰ intermediate [13]. D156 has been shown to interact via hydrogen bonding with C128, denoted as the DC gate [14]. The X-ray structure as well as theoretical calculations confirmed that the terminal groups of both amino acids are interconnected via a water molecule [10,15]. D156 is protonated in the dark state and deprotonates during the P₂³⁹⁰ to P₃⁵²⁰ transition concomitantly to the reprotonation of the Schiff base. Thus, D156 is the proton donor of the Schiff base in CrChR2 [13]. The distance from the DC gate to the Schiff base is too large for direct proton transfer. It was shown in Reference [10] that the nearby residue T127 may facilitate the reprotonation process. To evaluate this hypothesis, we set out to investigate variants in which T127 was replaced by alanine or serine.

Channel activity of the T127 variants was examined by electrophysiology and exhibited reduced conductance in the T127 variants. Molecular spectroscopy (UV/Vis, FTIR, Raman) was applied to scrutinize the role of T127 in the molecular mechanism of CrChR2. We report here the exceptionally high frequency of the Schiff base vibration in the T127A variant, indicating strong interaction between the protonated Schiff base and the carboxylic side chain of E123 in this variant. QM/MM calculations supported and extended the spectroscopic results with detailed atomistic descriptions of the hydrogen-bonded network surrounding the retinal Schiff base. We believe that the characterization of the threonine variants at the molecular level is an important step towards the understanding of the link between the protein's spectroscopic properties and its function as a light-activated cation channel.

2. Materials and Methods

2.1. Site-Directed Mutagenesis, Cloning, Expression and Purification of CrChR2

The experiments were executed with recombinant CrChR2, which consisted only of the membranous part containing amino acid residues 1–307 of channelrhodopsin-2 of *Chlamydomonas reinhardtii* (UniProt: Q8RUT8). Due to insertion of the corresponding coding region with sequences for a C-terminal 10xHis tag and a linker (aa AS) behind the alpha factor signal sequence of the vector pPIC 9K into the *EcoRI/NotI* sites, the expressed protein led to a N-terminal extension of aa YVEFH and a C-terminal extension of aa ASHHHHHHHHHH. Based on this construct, which is referred in the following as CrChR2-WT or simply WT, T127 was substituted by serine (T127S) or alanine residues (T127A). The substitutions were introduced with oligonucleotide-directed mutagenesis using PCR and verified by sequencing of the CrChR2 coding sequence. The CrChR2 variants were expressed and purified as described previously [16].

2.2. Molecular Spectroscopy

Time-resolved UV/Vis experiments were performed with a commercial flash photolysis unit (LKS80, Applied Photophysics, Leatherhead, Surrey, UK), as described previously [17]. Briefly, a 10 ns laser pulse (Nd:YAG, Quanta-Ray, Spectra-Physics) tuned to 450 nm by an optical parametric oscillator (OPTA) was used to induce the photocycle. The energy density per pulse was set to 3 mJ/cm². Five time traces were averaged at each wavelength with a repetition frequency of 0.33 Hz.

Samples used for FTIR spectroscopy were concentrated to ~4 mg/mL CrChR2 in an aqueous solution of 20 mM Hepes and 0.2% DM (n-decyl-β-D-maltopyranoside) at pH 7.4. For the FTIR experiments, approximately 8 μL of CrChR2 was dried on top of a BaF₂ window. The protein film was rehydrated with the saturated vapor phase of a glycerol/water mixture (2/8 w/w) [18] and placed into the FTIR spectrometer (Vertex 80v, Bruker, Rheinstetten, Germany). Time-resolved rapid-scan FTIR spectroscopy was employed to resolve intermediates with a time resolution of about 10 ms.

Resonance Raman experiments were performed essentially as described in Reference [19]. Briefly, 5 μL of concentrated sample (5–10 mg/mL) was dried and rehydrated on a quartz crucible and subsequently cooled to 80 K using a N₂ cryostat (Linkham). Rehydration occurred prior cooling via

vapor diffusion of 3 μl of either H_2O /glycerol or D_2O /glycerol mixtures (8/2 w/w) placed in the vicinity of the sample. The emission line at 457 nm of a diode-pumped solid-state (DPSS) laser (Changchun New Industries Optoelectronics Technology Co., Ltd., China) was used to induce Raman scattering.

2.3. Electrophysiology

Light-induced currents were recorded from oocytes in two-electrode voltage-clamp (TEVC) experiments after expression of the WT and the T127A or T127S variants for at least 3 days. To this end, in-vitro-synthesized RNA coding for a fusion protein of chop2 (residues 1 to 315) and egfp was injected into oocytes and incubated in oocyte Ringer (ORI, 90 mM NaCl, 2 mM KCl, 2 mM CaCl_2 , 1 mM MgCl_2 , 5 mM HEPES, pH 7.4) solution supplemented with 5 μM all-trans retinal. Oocytes were illuminated with light from a 75 W XBO lamp long-pass filtered at 420 nm in ORI. Currents of the T127 variants were normalized to the WT current amplitudes at -60 mV from oocytes recorded at the same day.

Time-resolved single turnover currents of the T127 variants were also recorded from HEK293 cells expressing the same fusion protein as in the oocyte recordings. Cells were illuminated with a single flash (20 ns) from an Excimer-laser pumped dye laser (coumarin 2, 450 nm). Traces were sampled at 50 kHz and filtered at 10 kHz. The displayed traces are averages of eight signals.

2.4. QM/MM Calculations

The structural model for hybrid quantum mechanics/molecular mechanics (QM/MM) calculations was based on the crystal structure of CrChR2 (PDB entry: 6EID [10]) with an all-trans conformation of the retinal protonated Schiff base (RSBH⁺). Titratable residues were modeled corresponding to the experimental pH and considering their local environment. Based on spectroscopic studies, the residue E90 was modeled in the neutral form and the counterions of RSBH⁺ (E123 and D253) were taken as negatively charged. The variants of CrChR2, T127A and T127S, were prepared with PyMol [20].

In order to account for the effect of T127 and its variants, we used a large QM region that comprised the RSBH⁺ side chains of E123, T127, A127, S127, C128, D253, K257, and two water molecules in the close vicinity of RSBH⁺. The hydrogen link atom was placed at the QM/MM boundary between the C δ and C ϵ atoms of K257, and between the C α and side chain atom of remaining residues. The QM region was treated at the B3LYP/cc-pVDZ level of theory [21]. Corrections for the dispersion effect were included with D3/B-J damping variant [22]. All the remaining atoms were described at the MM level using the AMBER ff14SB force field [23]. The vibrational frequencies were calculated at the same level of theory. A scaling factor of 0.97 was used [24]. However, the QM region in frequency calculations did not include the water molecules. Furthermore, the QM/MM model was used to calculate the excitation energies using the simplified TD-DFT approach developed by Grimme and coworkers [25]. All QM/MM calculations were carried out using ChemShell interfaced with the quantum chemistry program Orca with DL_POLY module for the force field [26].

3. Results

In the X-ray crystal structure of CrChR2, the distance between heavy atom pairs N(RSBH⁺) \cdots O(E123) and N(RSBH⁺) \cdots O(D253) is 2.81 and 3.24 \AA , respectively. The QM/MM geometry optimization leads to slight adjustments in the retinal binding pocket, which modifies the corresponding distances to 2.82 and 3.48 \AA . In WT, T127 was found to be hydrogen-bonded with E123 with an OH(T127) \cdots O(E123) distance of 1.70 \AA (Figure 2A). Upon T127S exchange, the hydrogen-bonding network was retained with a slightly reduced distance of 1.67 \AA between OH(T127S) \cdots O(E123) and an increased distance of 3.53 \AA between N(RSBH⁺) \cdots O(D253) (Figure 2B). The difference between serine and threonine residues is the absence of the methyl group at the C β position in the former. Lack of this bulky group in serine might cause a reduced steric effect responsible for its approach to E123. In contrast, the T127A variant was missing a proton-donating group (Figure 2C); therefore, E123 had only one hydrogen-bonding partner, namely the Schiff base. The distance between N(RSBH⁺) \cdots O(E123) remained the same (2.81 \AA), but the N–H bond length

was elongated by 0.016 Å (Table 1) because the proton is pulled more strongly towards E123 as a consequence of its altered hydrogen bonding.

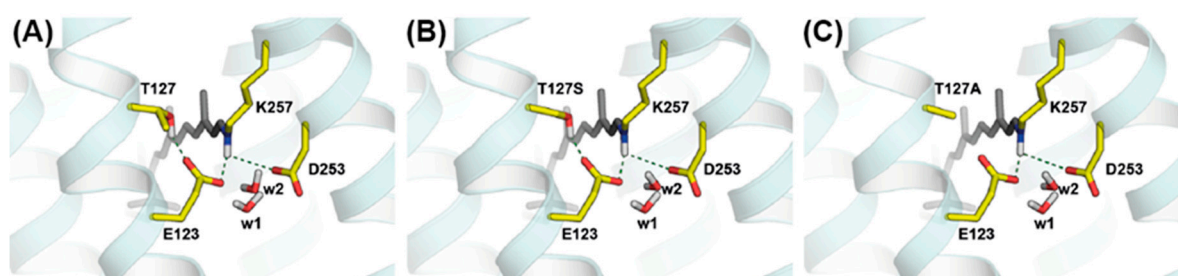


Figure 2. Optimized geometry of (A) CrChR2-WT, (B) T127S, and (C) T127A variants. The retinal Schiff base and side chains of the counterion complex are shown as grey and yellow sticks, respectively. Dotted lines correspond to the hydrogen-bonding network.

Table 1. Bond length in selected RSBH⁺ atom pairs, based on the hybrid quantum mechanics/molecular mechanics (QM/MM)-optimized geometries.

RSBH ⁺ Atom Pairs (Distances in Å)	WT	T127S	T127A
C=N	1.310	1.308	1.309
N-H	1.076	1.072	1.092

In CrChR2-WT, T127 was also found to be involved in a triad between O(E123), OH(T127), and S(C128). The corresponding distances in the optimized geometry were found to be 4.91 Å for O(E123)⋯S(C128) and 4.39 Å for OH(T127)⋯S(C128). In the T127S variant, the distance between O(E123)⋯S(C128) was slightly reduced to 4.88 Å, whereas the distance between OH(T127S)⋯S(C128) was increased to 4.47 Å. This indicated that the T127S variant led to a tighter network with the DC gate and the SB counterions. However, the T127A exchange perturbed the triad and decoupled the DC gate from the counterions, as the distance between O(E123)⋯S(C128) was increased to 4.95 Å.

3.1. Spectroscopic Properties of the Dark State of the T127 Variants of CrChR2

As T127 is part of the retinal binding pocket, we first examined the potential influence of the amino acid exchange on the electronic properties of the retinal. It was evident from comparison of the UV/Vis spectra (Figure 3, red and blue spectra) that both T-A and T-S amino acid exchanges shifted the visible absorption spectrum only slightly to the blue as compared to WT (black spectrum in Figure 3). The second derivative of the absorption spectra (bottom panel) resolved a blue shift of about 2 nm in the T127A variant as compared to the WT (similar to T127S, not shown). The vibronic fine structure of the electronic absorption spectrum was retained in the T127A and the T127S variants. The latter observation was different to the C128T variant, where a 20 nm redshift of the retinal absorption was accompanied by a loss in vibronic fine structure [27].

We also computed the excitation energies for the WT protein and the two variants. The results displayed in Table 2 showed virtually no alteration of the excitation energies, which agreed well with the experimental results (Figure 3). These results present an additional validation of our QM/MM model.

Table 2. Computed excitation energies at the sTD-DFT CAM-B3LYP/cc-pVDZ level of theory.

Model	WT	T127S	T127A
Excitation energy nm (eV)	389 (3.18)	392 (3.16)	388 (3.19)

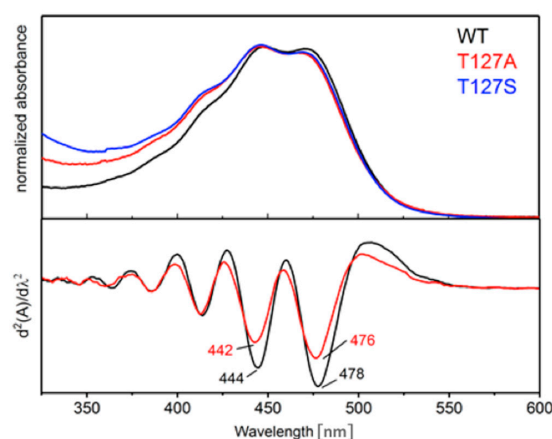


Figure 3. UV/Vis absorption spectra for the CrChR2-WT, T127A, and T127S variants. The second derivatives of the absorption spectra are displayed in the bottom panel; the second derivative of the T127S spectrum has been omitted for clarity as it overlaps with the T127A trace.

As the wavelength of the electronic absorption in the visible correlated with the C=C stretching vibration [28], the strongest band in the resonance Raman spectrum of the T127A variant (Figure 4, green trace) was 1557 cm^{-1} , slightly blue-shifted by 6 cm^{-1} with respect to the WT (Figure 5A, [29]). All of the other Raman bands were essentially the same as in the WT, except for the C=N–H vibration of the retinal Schiff base (Figure 5B). The frequency of the latter was observed at 1674 cm^{-1} for T127A, which is, to our knowledge, the highest frequency so far observed for any rhodopsin. It even outperformed the frequency of the Schiff base vibration in rhodopsin (1660 cm^{-1} , [30]). The C=N–H vibrational band was downshifted by 42 cm^{-1} upon H/D exchange, which was the largest isotope effect reported (Figure 4). In comparison, the C=N–H stretch in WT resonated with a frequency of 1657 cm^{-1} and a $\Delta\nu_{\text{H/D}} = 28\text{ cm}^{-1}$ was reported [29]. As the hydrogen bond between T127 and E123 was removed in the T127A variant (Figure 2C), the carboxylic side chain of E123 was able to form a stronger salt bridge with the retinal Schiff base, resulting in a 0.016 \AA elongated N–H bond (Table 1).

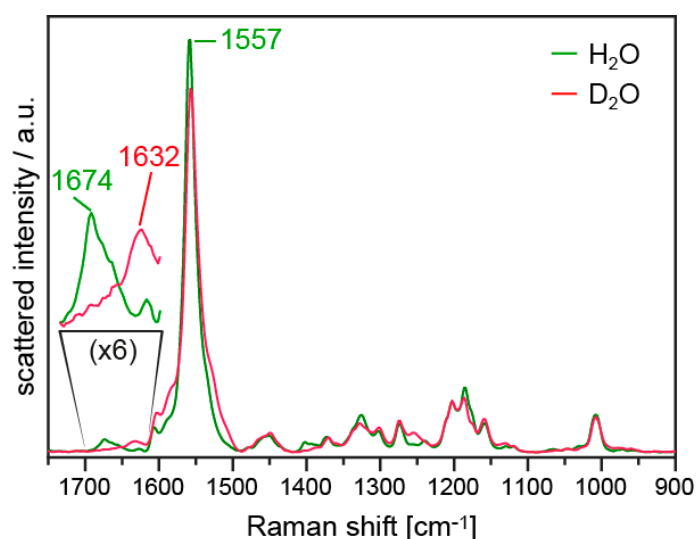


Figure 4. Resonance Raman spectra of the T127A variant in H_2O (green trace) and in D_2O (red trace). The indicated vibrational bands are discussed in the text.

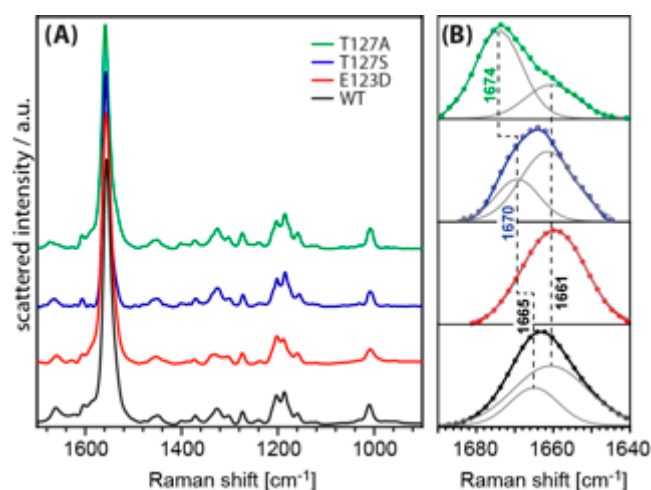


Figure 5. (A) Resonance Raman spectra of CrChR2-WT and the variants E123D, T127S, and T127A in H₂O. (B) Zoom-in of the frequency range of the Schiff base vibration after a three-point moving average smooth. Blue circles are the data points. Dashed grey lines are Gaussians fitted to the data points and continuous lines are sums of the fitted Gaussians.

Inspection of the vibrational band at 1674 cm⁻¹ revealed a strong asymmetry in the shape, with a pronounced shoulder at lower wavenumbers (green trace in Figure 5B). Consequently, the band was fitted by two Gaussians with frequency maxima at 1674 cm⁻¹ and 1661 cm⁻¹. Such heterogeneity in the retinal binding pocket has been suggested from molecular dynamics simulations on WT [31] to be a result of two rotamers of the side chain of E123. In one rotamer configuration, E123 was in direct hydrogen-bonding interaction with the protonated Schiff base, competing with a water molecule and D253. The other rotamer configuration positioned the carboxylic group of E123 in a remote position from the Schiff base. A water molecule or the carboxylic group of D253 can then form a hydrogen bond with the Schiff base proton. The resulting effect on the strength of the N–H bond of the Schiff base was acutely determined by Raman spectroscopy.

The vibrational band of the Schiff base in WT has so far been treated as a single vibration [32]. In light of our results for the T127A variant, we revisited the Raman spectrum of the WT (Figure 5, black trace). The slight asymmetry in band shape was again considered by fitting two Gaussians, resulting in maxima at 1665 cm⁻¹ and 1661 cm⁻¹.

From these results, we assigned the lower frequency of the C=N–H vibration at 1661 cm⁻¹ to the Schiff base being hydrogen-bonded to a water molecule and/or directly to D253. In this scenario, the substitution of T127 by A did not affect the frequency of the Schiff base vibration, as this residue did not interact directly with D253. This explained the low-frequency shoulder of the C=N–H band at 1661 cm⁻¹ which did not shift after amino acid exchange. The high-frequency band at 1674 cm⁻¹ in T127A corresponded to the population in which E123 was hydrogen bonded to the Schiff base and, with respect to the WT, lacked the hydrogen bond to the threonine (see Figure 2, right panel).

We tested this hypothesis by recording resonance Raman spectra for two other CrChR2 variants: T127S, where the hydroxyl group of the threonine side chain is conserved; and E123D, where the carboxylate side chain is shorter. In agreement with the WT and the T127A variant, all spectral features of the retinal chromophore were retained in the spectra of the T127S (blue traces in Figure 5) and E123D variants (red traces in Figure 5) with only minor differences. Analysis of the Schiff base vibration (Figure 5b) showed that the C=N–H band in E123D could be fitted sufficiently well with one Gaussian, whereas for T127S, two Gaussians were needed to fit the band. The band with a maximum at 1661 cm⁻¹ was present in both variants, supporting the hypothesis that this Schiff base vibration did not involve interaction with E123.

In T127S, where the exchange retained the hydroxyl group that is hydrogen-bonded to E123 (see Figure 2), the high-frequency shoulder of the peak was only slightly blue-shifted by 5 cm^{-1} , showing strong similarities to the C=N–H vibrational band of the WT. In E123D, however, the high frequency band was not present at all as a consequence of the shorter amino acid side chain length that prevented formation of a hydrogen bond with the Schiff base.

We focused our QM/MM calculations on the structure with the rotamer configuration of E123 in the upward orientation to be able to accept a hydrogen bond from the Schiff base proton. This configuration was in fact the one in which the C=N–H vibration exhibited the strongest effect in our T127 variants. Although the spectroscopic data showed that the hydrogen bond between the Schiff base and E123 was strongly strengthened upon replacement of T127, the distance between the Schiff base nitrogen and E123 was unchanged in the optimized QM/MM structure of the T127 variants. Thus, we went on to analyze the effect of the amino acid exchange on the length of the C=N and the N–H bonds of the Schiff base in our simulations (Table 1).

The length of the C=N bond was not significantly affected in T127S and T127A as compared to the WT. However, the hydrogen-bonding network in the vicinity of RSBH⁺ was found to have a notable effect, with the presence or absence of hydroxylic group in the sidechain at position 127. The difference in N–H bond length in WT and T127S was negligible ($\sim 0.004\text{ \AA}$), which was attributed to the hydrogen-bonding network facilitated by the hydroxylic side chain. In contrary, the absence of such a network in T127A increased the N–H bond length by 0.016 \AA . The longer N–H bond length in T127A was in line with our experimental findings that this variant accelerated deprotonation of RSBH⁺ (see Section 3.3) and it also supported the high frequency of the C=N–H vibration of 1674 cm^{-1} . QM/MM simulations yielded a frequency difference of 19 cm^{-1} between WT and the T127A variant (Table 3), which reproduced the frequency upshift upon removal of the hydroxylic group of threonine but overestimated the experimental difference of 9 cm^{-1} (Figure 5B). The exceptionally high frequency of the Schiff base C=N–H vibration in the T127A variant was, therefore, be assigned to the missing hydrogen-bond between A127 and E123 and the increase in distance between N(RSBH⁺) \cdots O(E123).

Table 3. Calculated vibrational frequencies of the C=N–H vibration using the QM/MM method.

Model	WT	T127S	T127A
Frequencies (cm^{-1})	1683 cm^{-1}	1683 cm^{-1}	1702 cm^{-1}

3.2. Channel Conductance of the T127 Variants

The role of T127 in the functional mechanism of the ion channel was scrutinized via electrophysiological experiments on WT and its T127 variants expressed in *Xenopus* oocytes. The T127A and the T127S variants showed a strong decrease in the current amplitude (for T127A: Figure 6A, red traces). On average, the variants exhibited only $9 \pm 1\%$ ($n = 29$ for T127A and $n = 18$ for T127S) of the WT currents. From the residual current, we determined the kinetics of the channel closing upon switching off the light (Figure 6B). It was slower than the WT ($\tau = 12\text{ ms}$), with $\tau = 22 \pm 3\text{ ms}$ ($n = 9$) for the T127A variant and with $\tau = 23 \pm 3\text{ ms}$ ($n = 9$) for the T127S variant.

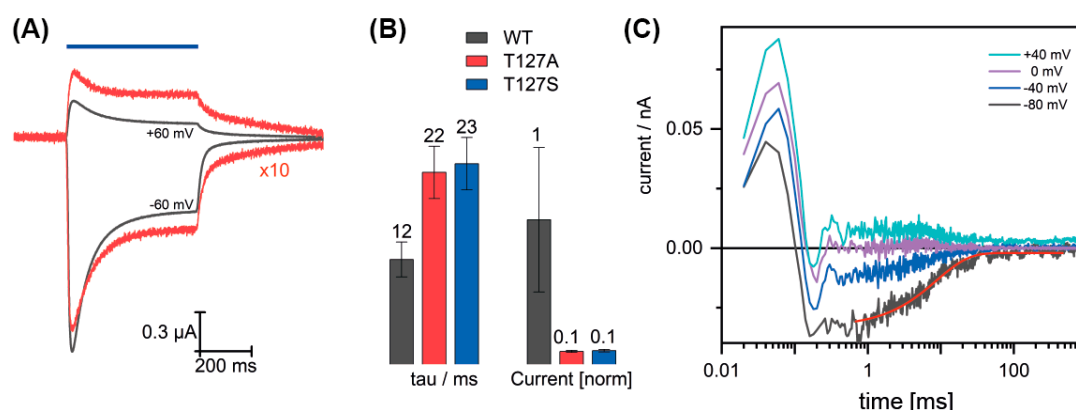


Figure 6. Two-electrode voltage-clamp (TEVC) recordings of CrChR2-WT, T127A, and T127S variants expressed in *Xenopus* oocytes. (A) Light-induced currents at -60 mV and $+60$ mV holding potential. The traces for the T127A variant (red) were scaled by a factor of 10 to compare to the WT (black). (B) Histogram of the current amplitudes and closing kinetics. Currents were normalized to the WT at -60 mV. Bars represent the mean and the s.e.m. ($n = 14$ for WT, $n = 29$ for T127A variant, and $n = 18$ for T127S variant). (C) Time-resolved currents from T127A in HEK293 cells. Raw data of an average of eight traces at -80 mV to $+40$ mV in steps of 40 mV. The red curve shows a single exponential fit of the current decay with a time constant of 10 ms.

In time-resolved experiments on the T127A variant expressed in HEK293 cells, only very small current amplitudes were recorded. Signals from eight kinetic traces were averaged (Figure 6C) to be able to determine the channel closing kinetics. Similarly to the E123T variant [33] we observed a very fast outward current independent of the holding potential, which monitored a vectorial charge transport within the first 200 μ s. The recovery kinetics after pulsed excitation exhibited single exponential behavior with a time constant of 10 ms, which was similar to the WT and consistent with our results from the TEVC recordings.

3.3. Influence of T127 on the Photocycle Kinetics

As the channel conductance was drastically reduced by the T127 replacement but the absorption spectrum of dark-state CrChR2 was hardly affected, we performed time-resolved UV/Vis spectroscopy (Figure 7). Excitation by a nanosecond laser pulse led to the depletion of the dark state of CrChR2, which was reflected by a loss of absorption at 470 nm (blue traces in Figure 7). The P_1^{500} state rose at times beyond the resolution of our experiment, but the decay was resolved at 530 nm (green traces). The rise of the blue-shifted P_2^{380} state with a deprotonated retinal Schiff base was recorded at 380 nm (red traces). Rise and decay of the succeeding P_3^{530} intermediate were observed at 530 nm and the latter correlated with channel closure in CrChR2 [34]. The kinetics of the desensitized state P_4^{480} were also observed at 530 nm.

The P_2^{380} state was formed faster in the T127A variant (Figure 7, top panel) and decayed slower than in the WT (Figure 7, bottom panel), i.e., the Schiff base deprotonated at an earlier stage and was reprotonated later. The kinetics of P_2^{380} rise in T127A had a half-life of $t_{1/2} = 0.7$ μ s, one order of magnitude faster than the rise of the P_2^{380} state in WT. The decay of this blue-shifted intermediate in T127A, with a $t_{1/2} = 9$ ms, was more than four times slower than in WT. The decay kinetics of the P_2^{380} state were altered at the expense of the P_3^{530} intermediate, which rose later and was significantly reduced in transient amplitude. This observation tallied the reduced channel conductance based on the correlation of the lifetimes of the open state and the P_3^{530} state. The decay of the non-conductive P_4^{480} state was not influenced by the T127A exchange. The less invasive replacement of threonine by serine in the T127S variant left the photocycle kinetics of CrChR2 unchanged (Figure 7, middle panel). Thus, we inferred that the hydroxyl group at position 127 was essential to a WT-like photoreaction, with a high accumulation of the late red-shifted intermediate P_3^{530} .

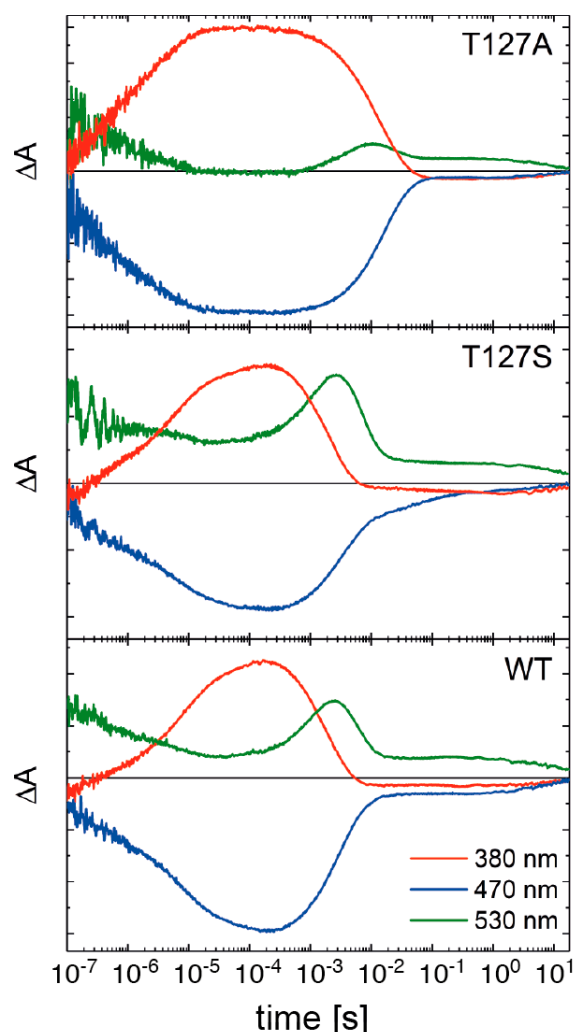


Figure 7. Kinetics in the UV/Vis range recorded after pulsed laser excitation (450 nm). Traces at 380 nm (red lines), 470 nm (blue), and 530 nm (green) are shown for each variant. While the T127A variant (top panel) showed a prolonged lifetime of the P_2^{380} state and reduced P_3^{530} formation, the T127S variant (middle panel) had very similar kinetics to the WT (bottom panel).

3.4. FTIR Difference Spectroscopy on the T127 Variants

FTIR spectroscopy was applied to gather information on the structural changes of the T127 variants (Figure 8). For comparison, difference spectra of CrChR2-WT were chosen at time points that represented mainly the intermediates P_2^{380} (300 μ s) and P_3^{530} (6.7 ms), and were compared to the difference spectra of the T127A and T127S variants recorded at 8.4 ms after pulsed excitation. At this time, the P_2^{380} intermediate was predominant in the variant with minor contributions from P_3^{530} and P_4^{480} intermediates.

The infrared difference spectra basically confirmed the observations made in the visible spectral range (Figure 6). The low accumulation of the P_3^{530} state in the T127A variant was observed by comparing the difference spectrum at 8.4 ms with the one at 6.7 ms of the WT. The band at 1737 cm^{-1} assigned to the deprotonation of the proton donor to the Schiff base, D156 [16], was reduced in intensity, which indicated low accumulation of the deprotonated D156 species. This observation was expected as soon as the lifetime of the P_2^{380} state (with deprotonated Schiff base) was extended, as here in the T127 variant. The negative band at 1556 cm^{-1} in the difference spectra of WT was due to the ethylenic stretching vibration of the retinal in ground-state ChR2 [32]. This band was hardly seen in T127A due

to spectral overlap by a positive contribution that is absent in the WT. Instead, a broad negative band at 1533 cm^{-1} was registered, which was a marker for the contribution of the P_4^{480} photoreaction [35].

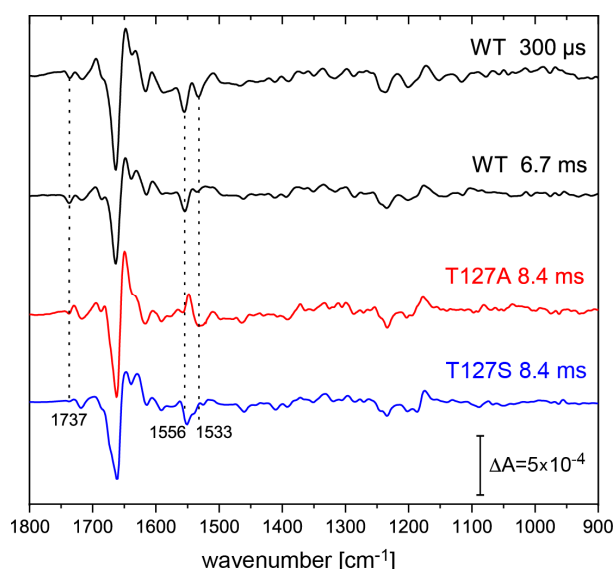


Figure 8. Time-resolved FTIR difference spectra of ChR2-WT (black spectra, taken from Reference [13]), T127A (red spectrum), and T127S variants (blue spectrum). The ChR2-WT spectrum at $300\ \mu\text{s}$ and $6.7\ \text{ms}$ was dominated by the P_2^{380} and P_3^{530} states, respectively. The spectra of the T127 variants were recorded at $8.4\ \text{ms}$, at which the P_2^{380} with smaller contributions of P_3^{530} was predominant.

4. Discussion

T127 of CrChR2 is localized in close vicinity to the retinal Schiff base and is hydrogen-bonded to E123 which, in turn, is the hydrogen bond acceptor of the Schiff base. The position of the threonine is also strategic for Schiff base reprotonation, as its hydroxylic group is supposed to be part of the pathway between the proton donor D156 and the Schiff base. There is no direct hydrogen-bonding network in the ground state that connects the RSBH^+ and D156, but it is only with the rise of the photocycle intermediate P_3^{530} that this connection is formed [13].

T127A substitution removed the hydroxylic group of the threonine, which affected the photocycle kinetics. The P_2^{380} intermediate, during the lifetime of which the Schiff base is deprotonated, had a ~ 10 times faster risetime, meaning that the deprotonation of the Schiff base was facilitated in this variant. The acceleration of the rise of the P_2^{380} intermediate may have been due to the stronger hydrogen-bonding interaction between the Schiff base and E123 that we reported in the present work.

The lifetime of the P_2^{380} state was longer in the T127A variant and, as a consequence, the accumulation of the subsequent intermediate P_3^{530} was very low. A longer lifetime of the state with a deprotonated Schiff base is a sign that the reprotonation pathway was blocked in T127A. The T127S variant conserved the hydroxyl group of the side chain, and we showed here that the photocycle kinetics were almost indistinguishable from the WT. We concluded, therefore, that the hydrogen-bonded network between D156 and the Schiff base, which is necessary for the reprotonation of the latter, involves the hydroxylic group of T127. The formation of this chain of hydrogen bonds is necessary for proton translocation and marks the transition between the P_2^{380} and P_3^{530} states.

T127 is important for the opening of the ion channel after light activation, since we have shown here that the T127A, as well as the more conservative T127S variants, showed less than 10% of the WT current in electrophysiology experiments. We note, though, that the reduced conductance may also have been related to lower expression yields of the variants in the different hosts (*Xenopus oocytes* and HEK cells). It has previously been shown that the channel closes with the decay of the P_3^{530} intermediate [36,37], but the channel opening is an optically silent transition in the visible range [38].

We confirmed from the present work that channel opening in CrChR2 is not related to changes in the photocycle kinetics as recorded by time-resolved UV/Vis spectroscopy. The T127S variant, in fact, showed WT-like photocycle kinetics, whereas a long-lived P_2^{380} intermediate occurred in the T127A variant with both variants exhibiting low channel conductance.

A threonine residue at this position was conserved for most of the cation- and anion-conducting channelrhodopsins. It is also present in BR [12,39], where exchanges to valine or alanine resulted in blue shifts in the absorption maxima by 146 nm and 28 nm, respectively, with minor effects on pumping activity [3]. By contrast, the exchange of threonine to serine and alanine in CrChR2 had only negligible effects on the electronic properties of the retinal chromophore, as registered by its visible absorption. This result is particularly interesting in light of the exceptionally high vibrational frequency recorded for the C=N–H vibration of the retinal Schiff base in T127A, as the hydrogen-bonding of the retinal Schiff base has been proposed to be a molecular determinant of the opsin shift [40].

QM/MM calculations showed nearly identical excitation energies for WT, T127S, and T127A variants. The same trend was also observed in the experimental absorption maxima of the retinal chromophore of CrChR2. However, a large shift of 19 cm^{-1} was calculated for the C=N–H vibration in the alanine variant, but no shift for the serine variant, again confirming the resonance Raman spectroscopic results. Since our QM/MM models were able to reproduce the relative trends in the UV/Vis and vibrational spectra of the variants, we considered these reliable for our analysis of the molecular changes. In the T127A variant, the hydrogen bond between the threonine and E123 was missing, affecting the hydrogen-bonding network around the Schiff base. To compensate for the missing hydrogen bond, the interaction between E123 and the Schiff base ($\text{N}(\text{RSBH}^+) \cdots \text{O}(\text{E123})$) increased, resulting in a longer N–H bond which manifested in the upshift of the C=N–H vibrational frequency. The elongation of the Schiff base N–H bond was 0.016 \AA , and possibly accelerates the deprotonation of the Schiff base in this variant. Hence, the stronger interaction between the Schiff base and E123 provided an explanation for the faster rise time of the P_2^{380} intermediate in the T127A variant, in a similar way to the D85E variant of bacteriorhodopsin [41].

Detailed analysis of the Schiff base vibration (coupled mode of the C=N stretching and the N–H bending vibration) by resonance Raman spectroscopy revealed the presence of two overlapping bands. The frequency shifts of these vibrational bands in the different variants were compared to the WT and their presence can be rationalized on the basis of the molecular model proposed in Reference [31]. In this model, the E123 side chain had one rotamer pointing towards the Schiff base and another rotamer pointing to a different hydrogen-bonding network that gave rise to two different vibrational bands of the C=N–H mode. This interpretation was supported by the band shape of the Schiff base vibration in the E123D variant, which was missing the high-frequency component. We can therefore lend support to the model of two rotamers of E123 in CrChR2, where a direct hydrogen bond with the Schiff base was formed in only one of the two configurations. The presence of two rotamer configurations may be essential for a voltage-sensing mechanism involving E123 [42]. While this seems to be a plausible scenario, further experimental evidence needs to be collected to support this model.

Author Contributions: Conceptualization, R.S. and J.H.; Funding acquisition, R.S. and J.H.; Investigation, D.E., N.K., M.S., C.B., R.K.K., K.H., D.H. and I.S.; Writing—original draft, R.S. and N.K.; Writing—review & editing, J.H. and M.S.

Funding: The research was funded by the German Research Foundation via the SFB-1078 projects B3 (to J.H.) and B4 (to R.S.). I.S. thanks the SFB 1078 for support within the Mercator program. R.K.K. acknowledges support from the Lady Davis Trust for Shunbrun postdoctoral fellowship. I.S. gratefully acknowledges funding by the European Research Council (ERC) under the European Union's Horizon 2020 research and innovation program (Grant No. 678169 "PhotoMutant").

Acknowledgments: The publication of this article was funded by Freie Universität Berlin.

Conflicts of Interest: The authors declare no conflict of interest.

References

1. Nagel, G.; Ollig, D.; Fuhrmann, M.; Kateriya, S.; Musti, A.M.; Bamberg, E.; Hegemann, P. Channelrhodopsin-1: A light-gated proton channel in green algae. *Science* **2002**, *296*, 2395–2398. [[CrossRef](#)] [[PubMed](#)]
2. Nagel, G.; Szellas, T.; Huhn, W.; Kateriya, S.; Adeishvili, N.; Berthold, P.; Ollig, D.; Hegemann, P.; Bamberg, E. Channelrhodopsin-2, a directly light-gated cation-selective membrane channel. *Proc. Natl. Acad. Sci. USA* **2003**, *100*, 13940–13945. [[CrossRef](#)] [[PubMed](#)]
3. Marti, T.; Otto, H.; Mogi, T.; Rosselet, S.J.; Heyn, M.P.; Khorana, H.G. Bacteriorhodopsin mutants containing single substitutions of serine or threonine residues are all active in proton translocation. *J. Biol. Chem.* **1991**, *266*, 6919–6927.
4. Rothschild, K.J.; He, Y.W.; Sonar, S.; Marti, T.; Khorana, H.G. Vibrational spectroscopy of bacteriorhodopsin mutants. Evidence that thr-46 and thr-89 form part of a transient network of hydrogen bonds. *J. Biol. Chem.* **1992**, *267*, 1615–1622. [[PubMed](#)]
5. Russell, T.S.; Coleman, M.; Rath, P.; Nilsson, A.; Rothschild, K.J. Threonine-89 participates in the active site of bacteriorhodopsin: Evidence for a role in color regulation and schiff base proton transfer. *Biochemistry* **1997**, *36*, 7490–7497. [[CrossRef](#)]
6. Pebay-Peyroula, E.; Rummel, G.; Rosenbusch, J.P.; Landau, E.M. X-ray structure of bacteriorhodopsin at 2.5 angstroms from microcrystals grown in lipidic cubic phases. *Science* **1997**, *277*, 1676–1681. [[CrossRef](#)]
7. Luecke, H.; Richter, H.T.; Lanyi, J.K. Proton transfer pathways in bacteriorhodopsin at 2.3 angstrom resolution. *Science* **1998**, *280*, 1934–1937. [[CrossRef](#)]
8. Kandori, H.; Kinoshita, N.; Yamazaki, Y.; Maeda, A.; Shichida, Y.; Needleman, R.; Lanyi, J.K.; Bizounok, M.; Herzfeld, J.; Raap, J.; et al. Structural change of threonine 89 upon photoisomerization in bacteriorhodopsin as revealed by polarized ftir spectroscopy. *Biochemistry* **1999**, *38*, 9676–9683. [[CrossRef](#)]
9. Kandori, H.; Yamazaki, Y.; Shichida, Y.; Raap, J.; Lugtenburg, J.; Belenky, M.; Herzfeld, J. Tight asp-85-thr-89 association during the pump switch of bacteriorhodopsin. *Proc. Natl. Acad. Sci. USA* **2001**, *98*, 1571–1576. [[CrossRef](#)]
10. Volkov, O.; Kovalev, K.; Polovinkin, V.; Borshchevskiy, V.; Bamann, C.; Astashkin, R.; Marin, E.; Popov, A.; Balandin, T.; Willbold, D.; et al. Structural insights into ion conduction by channelrhodopsin 2. *Science* **2017**, *358*, 8862. [[CrossRef](#)]
11. Hou, S.Y.; Govorunova, E.G.; Ntefidou, M.; Lane, C.E.; Spudich, E.N.; Sineshchekov, O.A.; Spudich, J.L. Diversity of chlamydomonas channelrhodopsins. *Photochem. Photobiol.* **2012**, *88*, 119–128. [[CrossRef](#)] [[PubMed](#)]
12. Govorunova, E.G.; Sineshchekov, O.A.; Rodarte, E.M.; Janz, R.; Morelle, O.; Melkonian, M.; Wong, G.K.-S.; Spudich, J.L. The expanding family of natural anion channelrhodopsins reveals large variations in kinetics, conductance, and spectral sensitivity. *Sci. Rep.* **2017**, *7*, 43358. [[CrossRef](#)] [[PubMed](#)]
13. Lorenz-Fonfria, V.A.; Resler, T.; Krause, N.; Nack, M.; Gossing, M.; Fischer von Mollard, G.; Bamann, C.; Bamberg, E.; Schlesinger, R.; Heberle, J. Transient protonation changes in channelrhodopsin-2 and their relevance to channel gating. *Proc. Natl. Acad. Sci. USA* **2013**, *110*, 1273–1281. [[CrossRef](#)] [[PubMed](#)]
14. Nack, M.; Radu, I.; Gossing, M.; Bamann, C.; Bamberg, E.; von Mollard, G.F.; Heberle, J. The dc gate in channelrhodopsin-2: Crucial hydrogen bonding interaction between c128 and d156. *Photochem. Photobiol. Sci.* **2010**, *9*, 194–198. [[CrossRef](#)] [[PubMed](#)]
15. Watanabe, H.C.; Welke, K.; Sindhikara, D.J.; Hegemann, P.; Elstner, M. Towards an understanding of channelrhodopsin function: Simulations lead to novel insights of the channel mechanism. *J. Mol. Biol.* **2013**, *425*, 1795–1814. [[CrossRef](#)] [[PubMed](#)]
16. Krause, N.; Engelhard, C.; Heberle, J.; Schlesinger, R.; Bittl, R. Structural differences between the closed and open states of channelrhodopsin-2 as observed by epr spectroscopy. *FEBS Lett.* **2013**, *587*, 3309–3313. [[CrossRef](#)]
17. Resler, T.; Schultz, B.J.; Lorenz-Fonfria, V.A.; Schlesinger, R.; Heberle, J. Kinetic and vibrational isotope effects of proton transfer reactions in channelrhodopsin-2. *Biophys. J.* **2015**, *109*, 287–297. [[CrossRef](#)]
18. Noguchi, T.; Sugiura, M. Flash-induced ftir difference spectra of the water oxidizing complex in moderately hydrated photosystem ii core films: Effect of hydration extent on s-state transitions. *Biochemistry* **2002**, *41*, 2322–2330. [[CrossRef](#)]

19. Schnedermann, C.; Muders, V.; Ehrenberg, D.; Schlesinger, R.; Kukura, P.; Heberle, J. Vibronic dynamics of the ultrafast all-trans to 13-cis photoisomerization of retinal in channelrhodopsin-1. *J. Am. Chem. Soc.* **2016**, *138*, 4757–4762. [CrossRef]
20. DeLano, W.L. *The PyMol Molecular Graphics System*; DeLano Scientific LLC: San Carlos, CA, USA, 2002.
21. Becke, A. Density-functional thermochemistry: The role of exchange. *J. Chem. Phys.* **1993**, *98*, 5648. [CrossRef]
22. Grimme, S.; Ehrlich, S.; Goerigk, L. Effect of the damping function in dispersion corrected density functional theory. *J. Comput. Chem.* **2011**, *32*, 1456–1465. [CrossRef] [PubMed]
23. Maier, J.A.; Martinez, C.; Kasavajhala, K.; Wickstrom, L.; Hauser, K.E.; Simmerling, C. Ff14sb: Improving the accuracy of protein side chain and backbone parameters from ff99sb. *J. Chem. Theory Comput.* **2015**, *11*, 3696–3713. [CrossRef] [PubMed]
24. Johnson, R. Nist Standard Reference Database Number 101. Available online: <http://cccbdb.nist.gov> (accessed on 1 October 2015).
25. Bannwarth, C.; Grimme, S. A simplified time-dependent density functional theory approach for electronic ultraviolet and circular dichroism spectra of very large molecules. *Comput. Theory Chem.* **2014**, *1040*, 45–53. [CrossRef]
26. Metz, S.; Kästner, J.; Sokol, A.A.; Keal, T.W.; Sherwood, P. Chem shell—A modular software package for qm/mm simulations. *Wires Comput. Mol. Sci.* **2014**, *4*, 101–110. [CrossRef]
27. Radu, I.; Bamann, C.; Nack, M.; Nagel, G.; Bamberg, E.; Heberle, J. Conformational changes of channelrhodopsin-2. *J. Am. Chem. Soc.* **2009**, *131*, 7313–7319. [CrossRef] [PubMed]
28. Aton, B.; Doukas, A.G.; Callender, R.H.; Becher, B.; Ebrey, T.G. Resonance raman studies of the purple membrane. *Biochemistry* **1977**, *16*, 2995–2999. [CrossRef]
29. Nack, M.; Radu, I.; Schultz, B.J.; Resler, T.; Schlesinger, R.; Bondar, A.N.; del Val, C.; Abbruzzetti, S.; Viappiani, C.; Bamann, C.; et al. Kinetics of proton release and uptake by channelrhodopsin-2. *FEBS Lett.* **2012**, *586*, 1344–1348. [CrossRef]
30. Narva, D.; Callender, R.H. On the state of chromophore protonation in rhodopsin: Implication for primary photochemistry in visual pigments. *Photochem. Photobiol.* **1980**, *32*, 273–276. [CrossRef]
31. Guo, Y.; Beyle, F.E.; Bold, B.M.; Watanabe, H.C.; Koslowski, A.; Thiel, W.; Hegemann, P.; Marazzi, M.; Elstner, M. Active site structure and absorption spectrum of channelrhodopsin-2 wild-type and c128t mutant. *Chem. Sci.* **2016**, *7*, 3879–3891. [CrossRef]
32. Nack, M.; Radu, I.; Bamann, C.; Bamberg, E.; Heberle, J. The retinal structure of channelrhodopsin-2 assessed by resonance raman spectroscopy. *FEBS Lett.* **2009**, *583*, 3676–3680. [CrossRef]
33. Lórenz-Fonfría, V.A.; Schultz, B.-J.; Resler, T.; Schlesinger, R.; Bamann, C.; Bamberg, E.; Heberle, J. Pre-gating conformational changes in the cheta variant of channelrhodopsin-2 monitored by nanosecond ir spectroscopy. *J. Am. Chem. Soc.* **2015**, *137*, 1850–1861. [CrossRef] [PubMed]
34. Lorenz-Fonfría, V.A.; Bamann, C.; Resler, T.; Schlesinger, R.; Bamberg, E.; Heberle, J. Temporal evolution of helix hydration in a light-gated ion channel correlates with ion conductance. *Proc. Natl. Acad. Sci. USA* **2015**, *112*, 5796–5804. [CrossRef] [PubMed]
35. Saita, M.; Pranga-Sellnau, F.; Resler, T.; Schlesinger, R.; Heberle, J.; Lorenz-Fonfría, V.A. Photoexcitation of the p4(480) state induces a secondary photocycle that potentially desensitizes channelrhodopsin-2. *J. Am. Chem. Soc.* **2018**, *140*, 9899–9903. [CrossRef] [PubMed]
36. Bamann, C.; Kirsch, T.; Nagel, G.; Bamberg, E. Spectral characteristics of the photocycle of channelrhodopsin-2 and its implication for channel function. *J. Mol. Biol.* **2008**, *375*, 686–694. [CrossRef] [PubMed]
37. Ernst, O.P.; Murcia, P.A.S.; Daldrop, P.; Tsunoda, S.P.; Kateriya, S.; Hegemann, P. Photoactivation of channelrhodopsin. *J. Biol. Chem.* **2008**, *283*, 1637–1643. [CrossRef] [PubMed]
38. Lórenz-Fonfría, V.A.; Heberle, J. Channelrhodopsin unchained: Structure and mechanism of a light-gated cation channel. *Biochim. Biophys. Acta Bioenerg.* **2014**, *1837*, 626–642. [CrossRef] [PubMed]
39. Del Val, C.; Royuela-Flor, J.; Milenkovic, S.; Bondar, A.N. Channelrhodopsins: A bioinformatics perspective. *Biochim. Biophys. Acta* **2014**, *1837*, 643–655. [CrossRef] [PubMed]
40. Fodor, S.; Gebhard, R.; Lugtenburg, J.; Bogomolni, R.; Mathies, R. Structure of the retinal chromophore in sensory rhodopsin i from resonance raman spectroscopy. *J. Biol. Chem.* **1989**, *264*, 18280–18283.

41. Heberle, J.; Oesterhelt, D.; Dencher, N.A. Decoupling of photo- and proton cycle in the asp85-> glu mutant of bacteriorhodopsin. *EMBO J.* **1993**, *12*, 3721–3727. [[CrossRef](#)]
42. Berndt, A.; Schoenenberger, P.; Mattis, J.; Tye, K.M.; Deisseroth, K.; Hegemann, P.; Oertner, T.G. High-efficiency channelrhodopsins for fast neuronal stimulation at low light levels. *Proc. Natl. Acad. Sci. USA* **2011**, *108*, 7595–7600. [[CrossRef](#)] [[PubMed](#)]



© 2019 by the authors. Licensee MDPI, Basel, Switzerland. This article is an open access article distributed under the terms and conditions of the Creative Commons Attribution (CC BY) license (<http://creativecommons.org/licenses/by/4.0/>).